JOURNAL OF THERMOPHYSICS AND HEAT TRANSFER
Vol. 25, No. 2, April–June 2011

Analytical and Numerical Solutions of Hyperbolic Heat Conduction in Cylindrical Coordinates

Mohsen Torabi* and Seyfolah Saedodin†
Semnan University, 35131-19111 Semnan, Iran

DOI: 10.2514/1.51395

The purpose of the present paper is to investigate the hyperbolic heat conduction subjected to heat flux boundary conditions. The governing equation is expressed in cylindrical coordinates. Equations are solved by deriving the analytical and the numerical solutions. The temperature layers and profiles of sample calculations are presented. It is found from these calculations that, although the presented numerical method is accurate in most cases, it has up to a 40% error in some cases compared with the analytical solution. Also, the temperature profiles from the sample calculations show that, as the Vernotte number increases, higher temperatures can be read during the process.

Nomenclature

A	=	constant coefficient
a_n	=	constant coefficient
A_1	=	matrix of constant coefficients for discretized equation
B	=	constant coefficient
B_1	=	matrix of constant coefficients for discretized equation
C	=	constant coefficient
c	=	specific heat, J/kg K
C_{fg}	=	constant coefficient
C_1	=	matrix of constant coefficients for discretized equation
c_1	=	constant coefficient
C_{12}	=	constant coefficient
c_2	=	constant coefficient
D	=	constant coefficient
$E^n_{i,j}$	=	error term of Taylor approximation
F	=	maximum value for f when $\kappa_{g,f}$ is real
f	=	nonnegative integer number
Fo	=	Fourier number, $\alpha t/L^2$
Fo_{final}	=	Fourier number at which the numerical algorithm stops
G	=	maximum value for g when $\kappa_{g,f}$ is real
g	=	nonnegative integer number
k	=	thermal conductivity, W/m K
L	=	height of the cylinder, m
M	=	square of cylinder aspect ratio, $(L/R)^2$
m	=	root of ratio of square of β to M, $\sqrt{\beta^2/M}$
q	=	incident heat flux, W/m^2
$\mathbf{q}$	=	heat flux vector, W/m^2
R	=	radius of cylinder, m
r	=	spatial coordinate, m
r_1	=	radius of area of application of boundary heat flux, m
T	=	temperature, K
t	=	temporal coordinate, s
T_i	=	initial temperature, K
$T_1(Fo)$	=	nondimensional temperature function employed as solution for ordinary differential Eq. (34) in analytical solution
T_∞	=	ambient temperature, K
Ve	=	Vernotte number, $\sqrt{\alpha\tau/L^2}$
$X(\xi)$	=	nondimensional temperature function employed as solution for ordinary differential Eq. (18) in analytical solution
$X_1(\xi)$	=	nondimensional temperature function employed as solution for ordinary differential Eq. (32) in analytical solution
z	=	spatial height coordinate, m
$Z(\omega)$	=	nondimensional temperature function employed as solution for ordinary differential Eq. (20) in analytical solution
$Z_1(\omega)$	=	nondimensional temperature function employed as solution for ordinary differential Eq. (30) in analytical solution
α	=	thermal diffusivity, m^2/s
β_n	=	eigenvalues
γ_f	=	eigenvalues
Δ	=	Laplace differential operator
ΔFo	=	increment of Fourier number in finite difference formulation
$\Delta\xi$	=	increment of the dimensionless spatial coordinate in ξ direction in finite difference formulation
$\Delta\omega$	=	increment of the dimensionless spatial coordinate in ω direction in finite difference formulation
η_g	=	eigenvalues
θ	=	dimensionless temperature, $k[(T - T_\infty)/Lq]$
$\vartheta_{g,f}$	=	combination of eigenvalues defined by Eq. (39)
$\kappa_{g,f}$	=	real parameter defined by Eq. (41a)
$(\kappa_{g,f})_i$	=	imaginary parameter defined by Eq. (41b)
ξ	=	dimensionless spatial radial coordinate
ξ_1	=	dimensionless radius of heat flux area of application
ρ	=	mass density, kg/m^3
τ	=	thermal relaxation time, s
$\phi(\xi, \omega)$	=	nondimensional temperature function employed in Eq. (11) as the solution for steady-state subproblem in analytical solution
$\psi(\xi, \omega, Fo)$	=	nondimensional temperature function employed in Eq. (11) as solution for homogeneous time-dependent subproblem in analytical solution
ω	=	dimensionless spatial height coordinate
∇	=	gradient operator

Received 29 June 2010; revision received 27 November 2010; accepted for publication 29 November 2010.

*Graduate M.S. Student, Department of Mechanical Engineering, Faculty of Engineering; Torabi_mech@yahoo.com.

†Assistant Professor, Department of Mechanical Engineering, Faculty of Engineering.

Subscripts

i = ith node in ξ direction
j = jth node in ω direction

Superscript

n = time step n

I. Introduction

DURING the past several years, there has been considerable research concerned with the departure from Fourier's heat conduction law when unsteady processes are involved. The motivation for this research was to investigate the paradox of infinite thermal wave speed. Current trends in bioheat transfer, nanoscale devices, and manufacturing processes have sparked renewed interest in the hyperbolic conduction law in order to investigate this paradox. Moreover, in situations that include extremely high temperature gradients, extremely large heat fluxes, or in the case of the near absolute zero temperatures, the heat propagation speeds are finite and the mode of conduction of heat is propagative and nondiffusive [1]. The non-Fourier heat conduction equation has received considerable attention, because of its wide applicability to engineering situations, such as solidifying processes [2], surface thermal processing by lasers [3], temperature control of superconductors [4], and laser surgery [5]. Hence, non-Fourier heat conduction has become one of the noteworthy subjects in the field of heat transfer.

To accommodate departure from the classical Fourier heat conduction model, Cattaneo [6] and Vernotte [7] independently proposed a modification of Fourier's law, which is now well known as Cattaneo–Vernotte's constitutive equation:

$$\mathbf{q} + \tau \frac{\partial \mathbf{q}}{\partial t} = -k \nabla T \tag{1}$$

Equation (1), combined with the conservation of energy, gives the hyperbolic heat transfer equation [8]:

$$\frac{\partial T}{\partial t} + \tau \frac{\partial^2 T}{\partial t^2} = \alpha \Delta T \tag{2}$$

Equation (2) is a hyperbolic partial differential equation and results in a thermal wave propagation speed, $\sqrt{\alpha/\tau}$, for $\tau > 0$.

Equation (2) has been experimentally validated for substances at very low temperatures, such as NaF at about 10 K [9] and Bi at 3.4 K [10]. More recently, non-Fourier heat conduction has been applied to predict temperatures for biological research. Zhou et al. [11] proposed a two-dimensional axisymmetric dual-phase-lag (DPL) model to describe heat transfer in living biological tissue with nonhomogeneous inner structures. Also, they developed a one-dimensional DPL bioheat transfer model to investigate the thermal response of living biological tissue to laser irradiation [12]. Xu et al. [13] derived the bioheat transfer equation in vector format and used the derived equation to study one-dimensional thermal damage of skin. But, non-Fourier heat conduction may introduce some unusual behavior and physically impossible solutions such as negative thermal energies. Korner and Bergmann [14] showed that the hyperbolic heat conduction equation (HHCE) predicts physically impossible solutions, especially negative thermal energies. Al-Nimr and Naji [15] demonstrated that the HHCE yields negative values for entropy, and this phenomenon violates the second law of thermodynamics. In recent years, Galovic et al. [16] showed that after the heat flux is switched off, the temperature falls below its initial value. They stated that if hyperbolic heat conduction were a theory based on the local equilibrium hypotheses, as the parabolic heat conduction is, this behavior would represent a violation of the second law of thermodynamics. Indeed, it has been pointed out in the literature that hyperbolic heat conduction is in contradiction with the local equilibrium hypothesis [17], so that no violation of the principles of thermodynamics occurs. López Molina et al. [18] showed that the negative temperature values are not always present and, in fact, these values depend on the relations between the duration of the dimensionless pulsed radio frequency (RF) power during RF heating of biological tissue, the dimensionless thermal relaxation time of the tissue, and the dimensionless position.

Various analytical and numerical solutions of the HHCE can be found in the literature. First, we review literature that has been applied to the HHCE analytically. There are many methods for solving the HHCE. Most researchers have solved the HHCE in one dimension [19–26]. Lewandowska and Malinowski [19] investigated the case of a thin film subjected to symmetric heating on both sides. Moosaie investigated hyperbolic heat conduction in a finite medium with an arbitrary source term [20] and arbitrary initial condition [21]. Tang and Araki [22] investigated non-Fourier fin problems under the periodic thermal boundary conditions. Zhang et al. [23] presented a non-Fourier model with heat sources. Saleh and Al-Nimr [24] employed Laplace transforms and used the software package MATLAB and the Taylor series to solve the one-dimensional HHCE. Jiang and Sousa [25] provided a completely analytical solution for hyperbolic heat conduction problems in a hollow homogeneous sphere with sudden temperature changes on its inner and outer surface. To the authors' knowledge, there is only one paper that solved the multidimensional HHCE analytically. Barletta and Zanchini [26] analytically investigated the HHCE using three-dimensional rectangular coordinates.

There is much literature that numerically solves the HHCE. Chen and Lin [27] applied a hybrid numerical technique to a problem with one spatial dimension. Yang [28] applied the modified Newton–Raphson method with the concept of future time to determine the boundary heat flux in a one-dimensional hyperbolic heat conduction problem. Zhou et al. [29] presented a thermal wave model for bioheat transfer, together with a seven-flux model for light propagation and a rate process equation for tissue damage. Huang and Lin [30] solved an inverse one-dimensional hyperbolic heat conduction problem by an iterative regularization method. Yang [31] applied a forward difference method to solve the two-dimensional HHCE. Also, he derived the stability conditions for the problem. Babaei and Chen [32] investigated hyperbolic heat conduction in a functionally graded hollow cylinder. They assumed that, except for uniform thermal relaxation time, all other material properties of the cylinder were varying along the radial direction. Although the validity of various non-Fourier models is debatable, no ultimate conclusion has been drawn at present due to the complexity of various heat transfer systems.

The pursuit of analytical solutions for the HHCE is of intrinsic scientific interest. In this paper, both analytical and numerical expressions for the temperature field are obtained for a cylinder. Therefore, we solve the HHCE in cylindrical coordinates. In fact, the two-dimensional analytical solution of the problem is obtained by

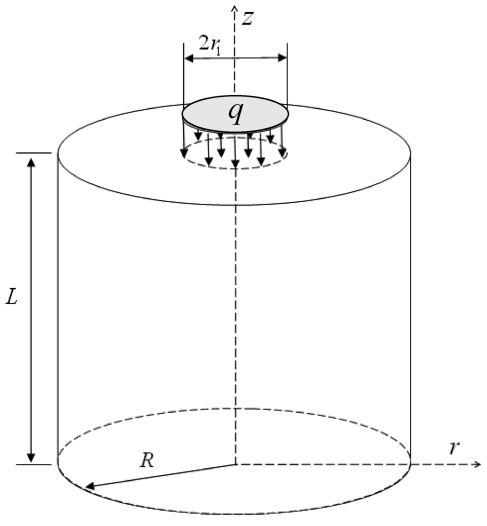

Fig. 1 Cylinder configuration.

Table 1 First eight values of β_n for $M = 16$

n	β
1	38.4772
2	88.3212
3	138.4596
4	188.6645
5	238.8946
6	289.1370
7	339.3861
7	389.6395

employing the method of separation of variables. The theoretical value of the analytical solution presented in this paper manuscript is that it can be used as a benchmark for verifying new numerical simulation techniques in this field. In addition, the two-dimensional numerical solution of the problem is obtained by employing the implicit finite difference method (FDM). Also, we present sample calculations for temperature distributions and profiles.

II. Problem Statement

Consider a cylinder, as shown in Fig. 1. A heat flux is applied normally to the upper surface ($z = L$) of the cylinder but only for $r \le r_1$.

A. Governing Differential Equation

For this case, without heat generation, the two-dimensional governing HHCE can be expressed as

$$\frac{1}{\alpha}\frac{\partial T}{\partial t} + \frac{\tau}{\alpha}\frac{\partial^2 T}{\partial t^2} = \frac{\partial^2 T}{\partial r^2} + \frac{1}{r}\frac{\partial T}{\partial r} + \frac{\partial^2 T}{\partial z^2} \tag{3}$$

B. Boundary Conditions

For this case, the boundary conditions are

$$\frac{\partial T}{\partial r}(0, z, t) = 0 \tag{4a}$$

$$T(R, z, t) = T_\infty \tag{4b}$$

$$T(r, 0, t) = T_\infty \tag{4c}$$

$$k\frac{\partial T}{\partial z}(r, L, t) = \begin{cases} q & r < r_1 \\ 0 & r > r_1 \end{cases} \tag{4d}$$

C. Initial Conditions

Consider the solid to be initially at the ambient temperature. Then,

$$T_i = T_\infty \tag{5}$$

Hence, the initial conditions are

$$T(r, z, 0) = T_\infty \tag{6a}$$

$$\frac{\partial T}{\partial t}(r, z, 0) = 0 \tag{6b}$$

III. Analytical Solution

For convenience in the subsequent analysis, we introduce the following dimensionless quantities:

$$\theta = k\frac{T - T_\infty}{Lq}, \quad \xi = \frac{r}{R}, \quad \omega = \frac{z}{L}, \quad Fo = \frac{\alpha t}{L^2}, \quad Ve = \sqrt{\frac{\alpha\tau}{L^2}}, \quad M = \left(\frac{L}{R}\right)^2, \quad \xi_1 = \frac{r_1}{R} \tag{7}$$

By introducing the dimensionless quantities, the normalized temperature of the cylinder obeys

$$Ve^2\frac{\partial^2\theta}{\partial Fo^2} + \frac{\partial\theta}{\partial Fo} = M\frac{\partial^2\theta}{\partial\xi^2} + \frac{M}{\xi}\frac{\partial\theta}{\partial\xi} + \frac{\partial^2\theta}{\partial\omega^2} \tag{8}$$

Also, the boundary conditions are

$$\frac{\partial\theta}{\partial\xi}(0, \omega, Fo) = 0 \tag{9a}$$

$$\theta(1, \omega, Fo) = 0 \tag{9b}$$

$$\theta(\xi, 0, Fo) = 0 \tag{9c}$$

$$\frac{\partial\theta}{\partial\omega}(\xi, 1, Fo) = \begin{cases} 1 & \xi \le \xi_1 \\ 0 & \xi > \xi_1 \end{cases} \tag{9d}$$

and the initial conditions are

$$\frac{\partial\theta}{\partial Fo}(\xi, \omega, 0) = 0 \tag{10a}$$

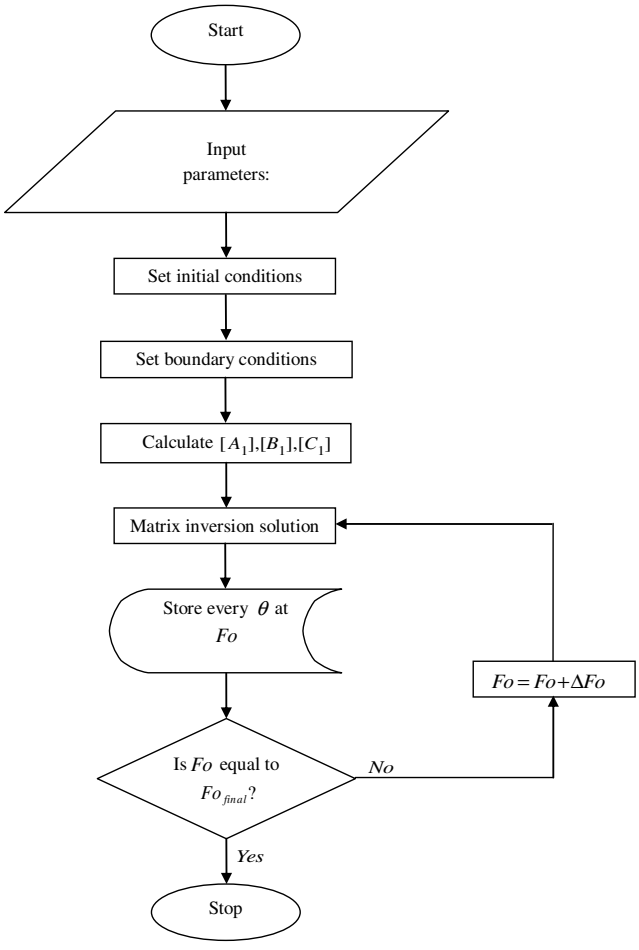

Fig. 2 Flowchart of numerical solution.

$$\theta(\xi, \omega, 0) = 0 \tag{10b}$$

If we want to apply the well-known separation-of-variables method, we should first split up Eq. (8) with the boundary [Eq. (9)] and the initial conditions [Eq. (10)] into a set of simpler problems. Carslaw and Jaeger [33] and Özisik [34] determined the solution of Eq. (8) from

$$\theta(\xi, \omega, Fo) = \psi(\xi, \omega, Fo) + \phi(\xi, \omega) \tag{11}$$

where the temperature $\phi(\xi, \omega)$ is taken as the solution of the following:

$$M\frac{\partial^2\phi}{\partial\xi^2} + \frac{M}{\xi}\frac{\partial\phi}{\partial\xi} + \frac{\partial^2\phi}{\partial\omega^2} = 0 \tag{12}$$

$$\frac{\partial}{\partial\xi}\phi(0, \omega) = 0 \tag{13a}$$

$$\phi(1, \omega) = 0 \tag{13b}$$

$$\phi(\xi, 0) = 0 \tag{13c}$$

$$\frac{\partial}{\partial\omega}\phi(\xi, 1) = \begin{cases} 1 & \xi \le \xi_1 \\ 0 & \xi > \xi_1 \end{cases} \tag{13d}$$

and the temperature $\psi(\xi, \omega, Fo)$ is taken as the solution of

$$Ve^2\frac{\partial^2\psi}{\partial Fo^2} + \frac{\partial\psi}{\partial Fo} = M\frac{\partial^2\psi}{\partial\xi^2} + \frac{M}{\xi}\frac{\partial\psi}{\partial\xi} + \frac{\partial^2\psi}{\partial\omega^2} \tag{14}$$

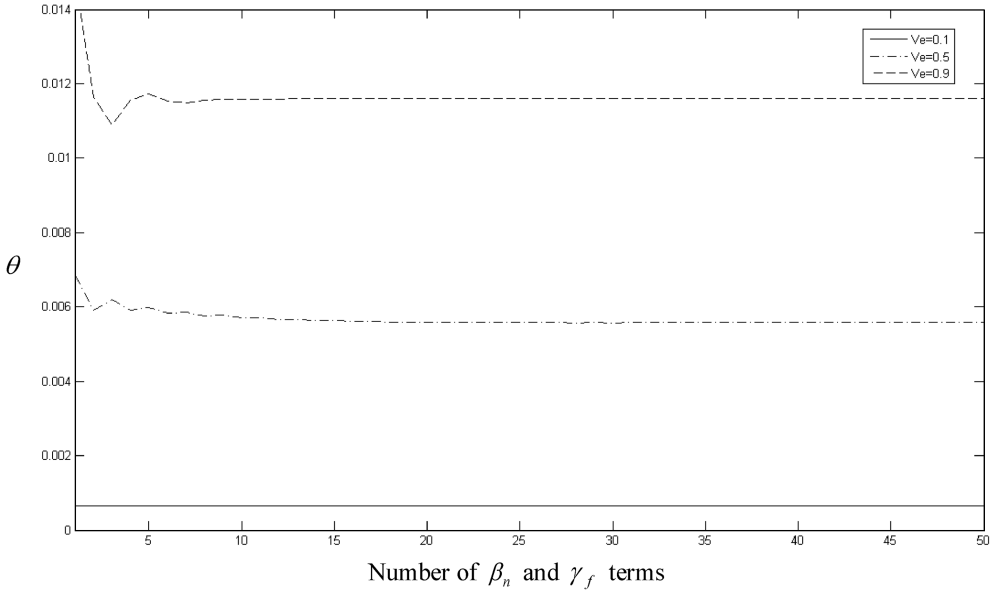

a) Temperature as a function of number of β_n and γ_f terms when first 350 values of η_g were used

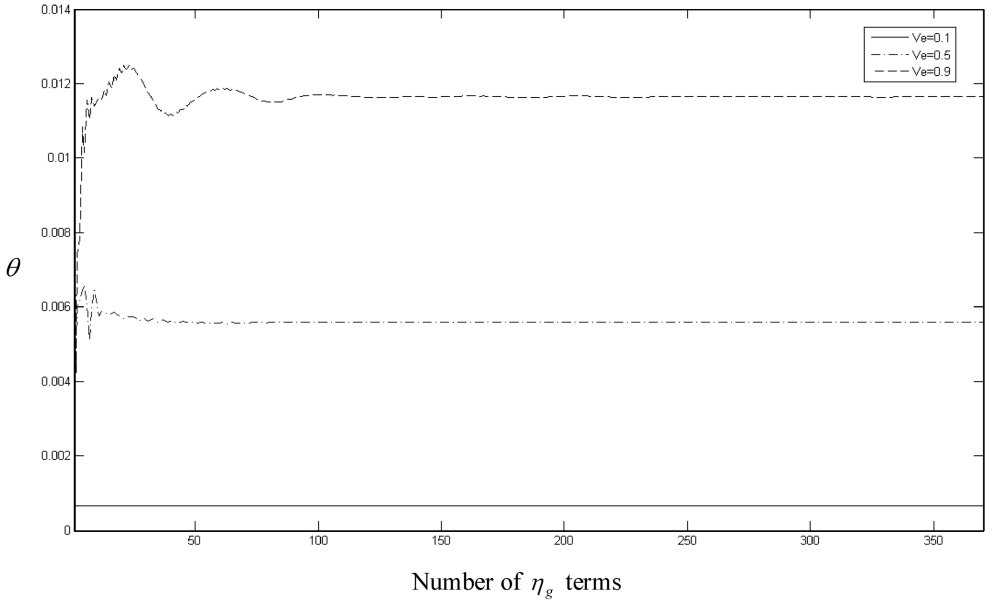

b) Temperature as a function of number of η_g terms when first 350 values of β_n and γ_f were used

Fig. 3 Temperature convergence for the specific point with $\xi = 0$, $\omega = 0.5$, $Ve = 0.7$, $Fo = 0.5$, $\xi_1 = 0.5$, and $M = 16$.

$$\frac{\partial}{\partial \xi}\psi(0,\omega,Fo)=0 \tag{15a}$$

$$\psi(1,\omega,Fo)=0 \tag{15b}$$

$$\psi(\xi,0,Fo)=0 \tag{15c}$$

$$\frac{\partial}{\partial \omega}\psi(\xi,1,Fo)=0 \tag{15d}$$

$$\frac{\partial}{\partial Fo}\psi(\xi,\omega,0)=0 \tag{15e}$$

$$\psi(\xi,\omega,0)=-\phi(\xi,\omega) \tag{15f}$$

Solving Eq. (12), we use the following separation:

$$\phi(\xi,\omega)\equiv X(\xi)Z(\omega) \tag{16}$$

By substituting Eq. (16) into Eq. (12) and rearranging,

$$M\left(\frac{1}{X}\frac{\mathrm{d}^2X}{\mathrm{d}\xi^2}+\frac{1}{X\xi}\frac{\mathrm{d}X}{\mathrm{d}\xi}\right)=-\frac{1}{Z}\frac{\mathrm{d}^2Z}{\mathrm{d}\omega^2}=\pm\beta^2 \tag{17}$$

Here, $-\beta^2$ is suitable for our problem. Finally, the problem can be separately expressed in the ξ and ω directions as follows:

$$\frac{\mathrm{d}^2X}{\mathrm{d}\xi^2}+\frac{1}{\xi}\frac{\mathrm{d}X}{\mathrm{d}\xi}+m^2X=0 \tag{18}$$

$$\frac{\mathrm{d}}{\mathrm{d}\xi}X(0)=0 \tag{19a}$$

$$X(1)=0 \tag{19b}$$

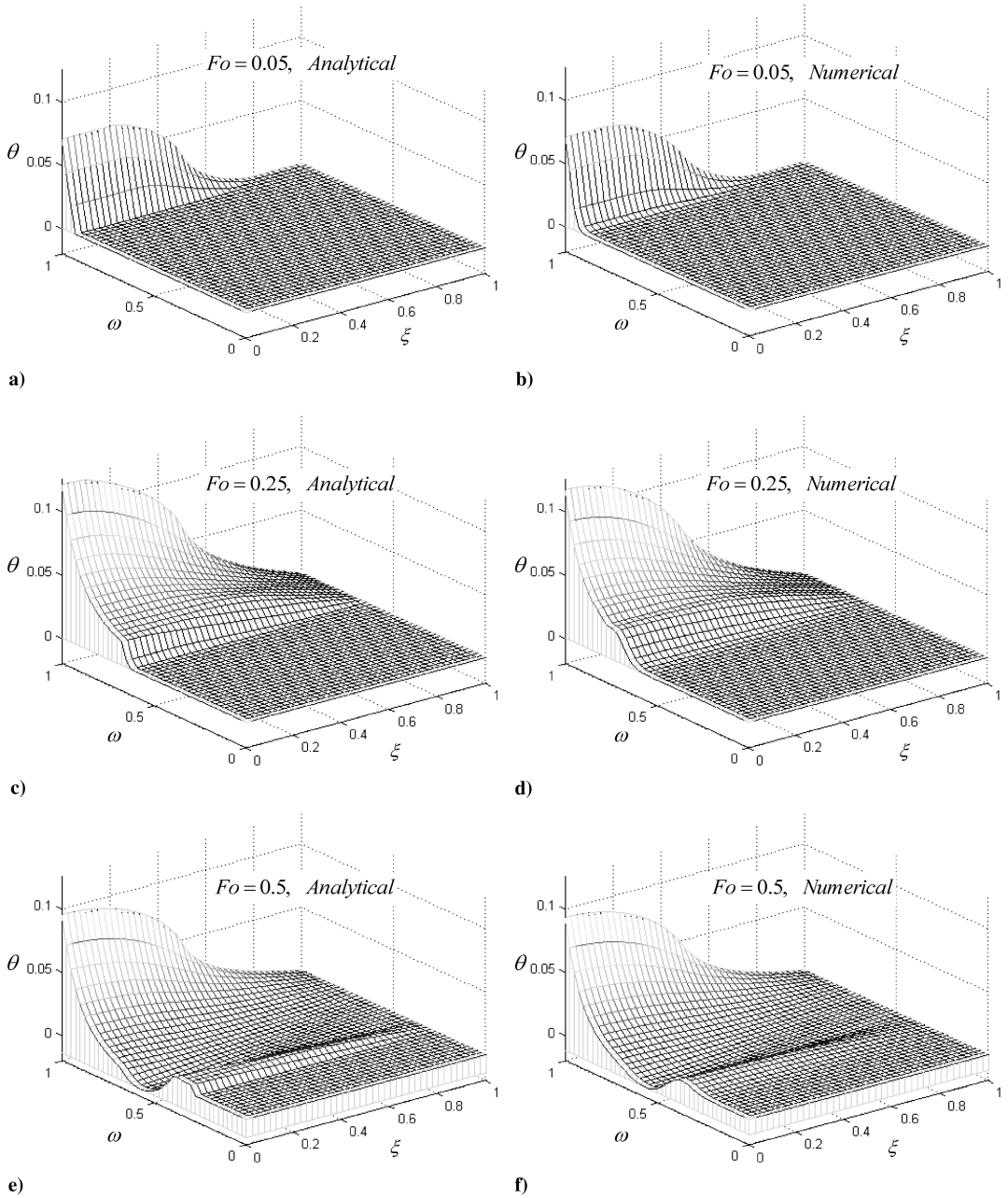

Fig. 4 Surface temperature evolution with $Ve = 0.7$, $\xi_1 = 0.5$, and $M = 16$ for non-Fourier model.

$$\frac{d^2Z}{d\omega^2} - \beta^2 Z = 0 \tag{20}$$

$$Z(0) = 0 \tag{21}$$

where

$$m^2 = \frac{\beta^2}{M} \tag{22}$$

Solving Eqs. (18) and (20), using Eqs. (19) and (21), yields

$$X(\xi) = CJ_0(\xi m_n) \tag{23}$$

$$Z(\omega) = B\sinh(\beta_n \omega) \tag{24}$$

where β_n are eigenvalues of $J_0(\beta_n/\sqrt{M}) = 0$. The first eight eigenvalues are given in Table 1 for $M = 16$. By substituting Eqs. (23) and (24) into Eq. (16), we obtain following solution for Eq. (12):

$$\phi(\xi, \omega) = \sum_{n=1}^{\infty} a_n \sinh(\beta_n \omega) J_0(m_n \xi) \tag{25}$$

Using the boundary condition [Eq. (13d)] and the orthogonality condition, we find the following:

$$a_n \beta_n \cosh \beta_n = \frac{\int_0^{\xi_1} \xi J_0(m_n \xi)\, d\xi}{\int_0^1 \xi J_0^2(m_n \xi)\, d\xi} \tag{26}$$

Solving Eq. (26), the constant a_n is given as

$$a_n = \frac{2\xi_1 J_1[(\beta_n/\sqrt{M})\xi_1]}{(\beta_n^2/\sqrt{M})\cosh \beta_n [J_1(\beta_n^2/\sqrt{M})]^2} \tag{27}$$

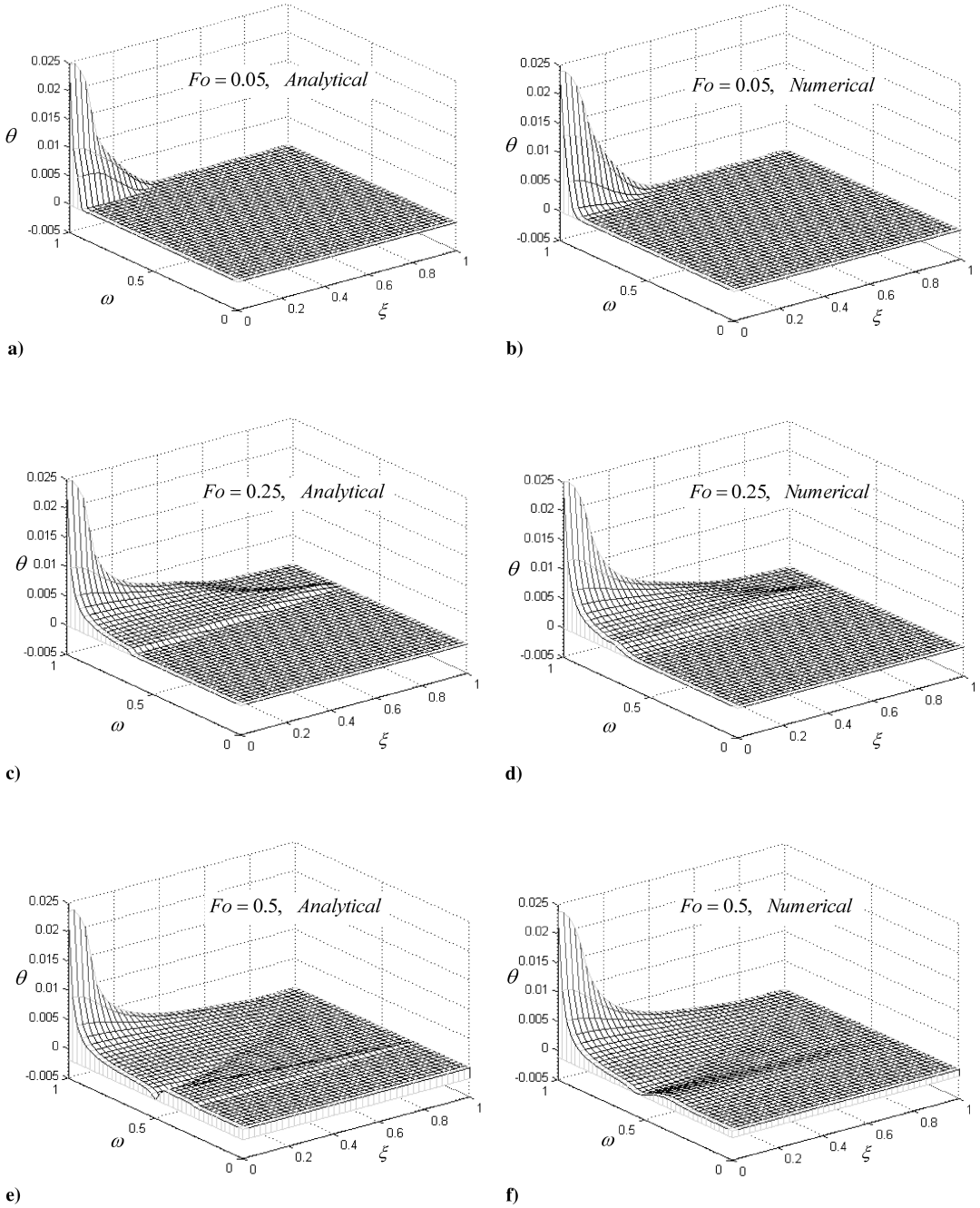

Fig. 5 Surface temperature evolution with $Ve = 0.7$, $\xi_1 = 0.1$, and $M = 16$ for non-Fourier model.

To solve Eq. (14), we should use the following separation:

$$\psi(\xi, \omega, Fo) \equiv X_1(\xi)Z_1(\omega)T_1(Fo) \tag{28}$$

By substituting Eq. (28) into Eq. (14) and rearranging, we find

$$\frac{Ve^2}{T_1}\frac{\mathrm{d}^2T_1}{\mathrm{d}Fo^2} + \frac{1}{T_1}\frac{\mathrm{d}T_1}{\mathrm{d}Fo} = M\left(\frac{1}{X_1}\frac{\mathrm{d}^2X_1}{\mathrm{d}\xi^2} + \frac{1}{X_1\xi}\frac{\mathrm{d}X_1}{\mathrm{d}\xi}\right) + \frac{1}{Z_1}\frac{\mathrm{d}^2Z_1}{\mathrm{d}\omega^2} = \pm\eta^2 \pm \gamma^2 \tag{29}$$

Here, $-\eta^2$ is suitable for our problem. Finally, the problem separately expressed in the ξ,ω, and Fo coordinates is as follows:

$$\frac{\mathrm{d}^2Z_1}{\mathrm{d}\omega^2} + \eta^2 Z_1 = 0 \tag{30}$$

$$Z_1(0) = 0 \tag{31a}$$

$$\frac{\mathrm{d}}{\mathrm{d}\omega}Z_1(1) = 0 \tag{31b}$$

$$\frac{\mathrm{d}^2X_1}{\mathrm{d}\xi^2} + \frac{1}{\xi}\frac{\mathrm{d}X_1}{\mathrm{d}\xi} + \frac{\gamma^2}{M}X_1 = 0 \tag{32}$$

$$\frac{\mathrm{d}}{\mathrm{d}\xi}X_1(0) = 0 \tag{33a}$$

$$X_1(1) = 0 \tag{33b}$$

$$Ve^2\frac{\mathrm{d}^2T_1}{\mathrm{d}Fo^2} + \frac{\mathrm{d}T_1}{\mathrm{d}Fo} + (\eta^2 + \gamma^2)T_1 = 0 \tag{34}$$

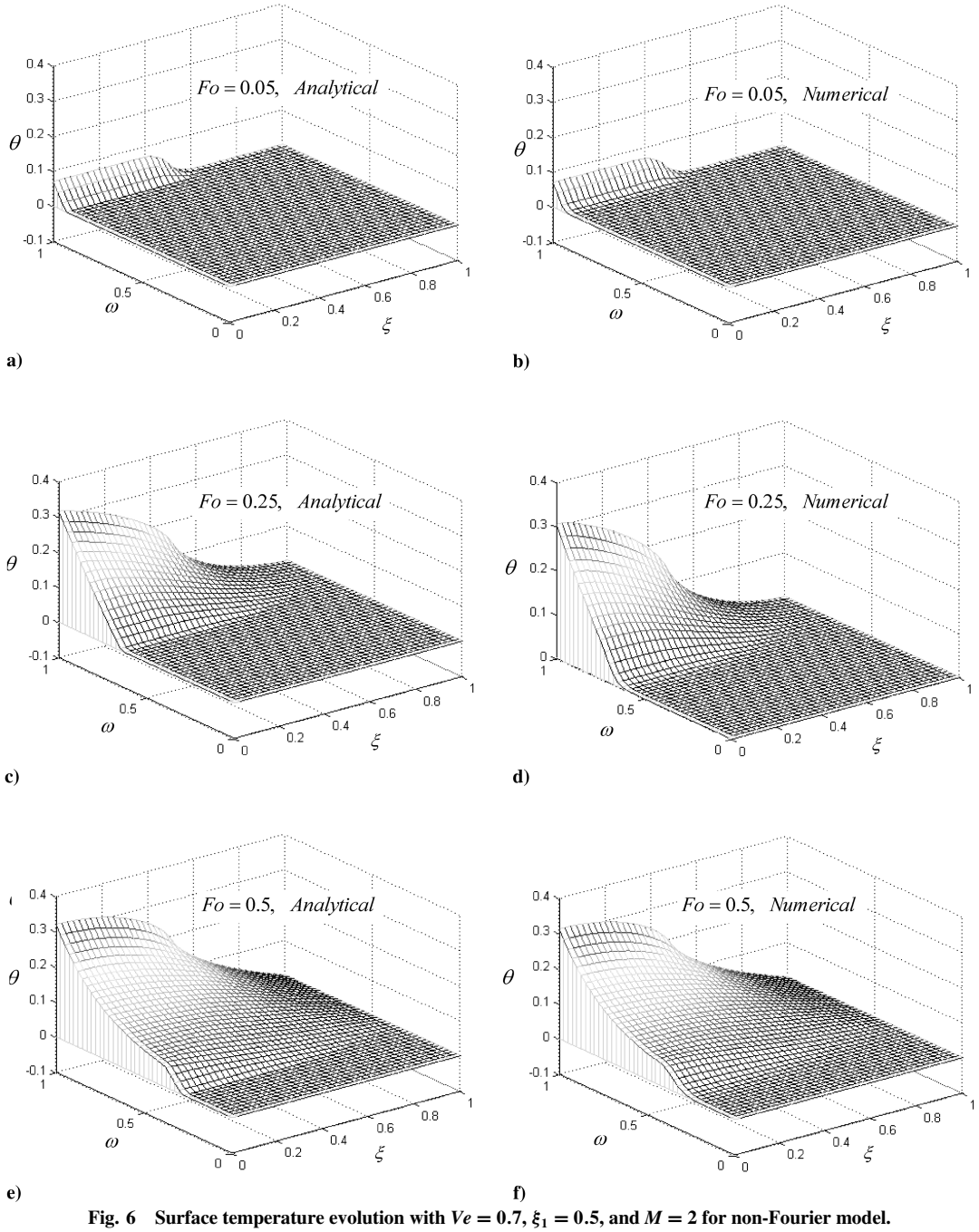

Fig. 6 Surface temperature evolution with $Ve = 0.7$, $\xi_1 = 0.5$, and $M = 2$ for non-Fourier model.

$$\frac{\mathrm{d}}{\mathrm{d}Fo}T_1(0) = 0 \tag{35}$$

Solving Eqs. (30), (32), and (34) using Eqs. (31), (33), and (35) gives

$$Z_1(\omega) = A\sin(\eta_g\omega) \tag{36}$$

$$X_1(\xi) = BJ_0\left(\frac{\gamma_f}{\sqrt{M}}\xi\right) \tag{37}$$

$$T_{1g,f}(Fo) = C_{12}\begin{cases} e^{-Fo/2Ve^2}\left\{\frac{1}{\kappa_{g,f}}\sinh\left(\frac{\kappa_{g,f}Fo}{2Ve^2}\right) + \cosh\left(\frac{\kappa_{g,f}Fo}{2Ve^2}\right)\right\} & \kappa_{g,f} = \text{real} \\ e^{-Fo/2Ve^2}\left\{\frac{1}{(\kappa_{g,f})_i}\sin\left(\frac{(\kappa_{g,f})_iFo}{2Ve^2}\right) + \cos\left(\frac{(\kappa_{g,f})_iFo}{2Ve^2}\right)\right\} & \kappa_{g,f} = i(\kappa_{g,f})_i \end{cases} \tag{42}$$

where η_g and γ_f are eigenvalues of $\cos\eta_g = 0$ and $J_0(\gamma_f/\sqrt{M}) = 0$, respectively. For Eq. (34), if $1 - 4Ve^2\vartheta_{g,f}^2 > 0$, we obtain

$$T_{1g,f}(Fo) = e^{-Fo/2Ve^2}\left[c_1\sinh\left(\frac{\kappa_{g,f}Fo}{2Ve^2}\right) + c_2\cosh\left(\frac{\kappa_{g,f}Fo}{2Ve^2}\right)\right] \tag{38}$$

where

$$\vartheta_{g,f}^2 = \eta_g^2 + \gamma_f^2 \tag{39}$$

and if $1 - 4Ve^2\vartheta_{g,f}^2 < 0$,

$$T_{1g,f}(Fo) = e^{-Fo/2Ve^2}\left[c_1\sin\left(\frac{(\kappa_{g,f})_iFo}{2Ve^2}\right) + c_2\cos\left(\frac{(\kappa_{g,f})_iFo}{2Ve^2}\right)\right] \tag{40}$$

where

$$\kappa_{g,f} = \sqrt{1 - 4Ve^2\vartheta_{g,f}^2} \tag{41a}$$

$$\kappa_{g,f} = i(\kappa_{g,f})_i \tag{41b}$$

By substituting Eqs. (38) and (40) into Eq. (35) to eliminate c_1 or c_2,

Substituting Eqs. (36), (37), and (42) into Eq. (28), the following equation for $\psi(\xi, \omega, Fo)$ is obtained:

$$\begin{aligned}\psi(\xi,\omega,Fo) = {} & \sum_{f=1}^{F}\sum_{g=0}^{G} C_{fg}\exp\left(-\frac{Fo}{2Ve^2}\right)\left[\frac{1}{\kappa_{g,f}}\sinh\left(\frac{\kappa_{g,f}Fo}{2Ve^2}\right)\right. \\ & \left. + \cosh\left(\frac{\kappa_{g,f}Fo}{2Ve^2}\right)\right]\sin(\eta_g\omega)J_0\left(\frac{\gamma_f}{\sqrt{M}}\xi\right) \\ & + \sum_{f=F+1}^{\infty}\sum_{g=G+1}^{\infty} C_{fg}\exp\left(-\frac{Fo}{2Ve^2}\right)\left[\frac{1}{(\kappa_{g,f})_i}\sin\left(\frac{(\kappa_{g,f})_iFo}{2Ve^2}\right)\right. \\ & \left. + \cos\left(\frac{(\kappa_{g,f})_iFo}{2Ve^2}\right)\right]\sin(\eta_g\omega)J_0\left(\frac{\gamma_f}{\sqrt{M}}\xi\right)\end{aligned} \tag{43}$$

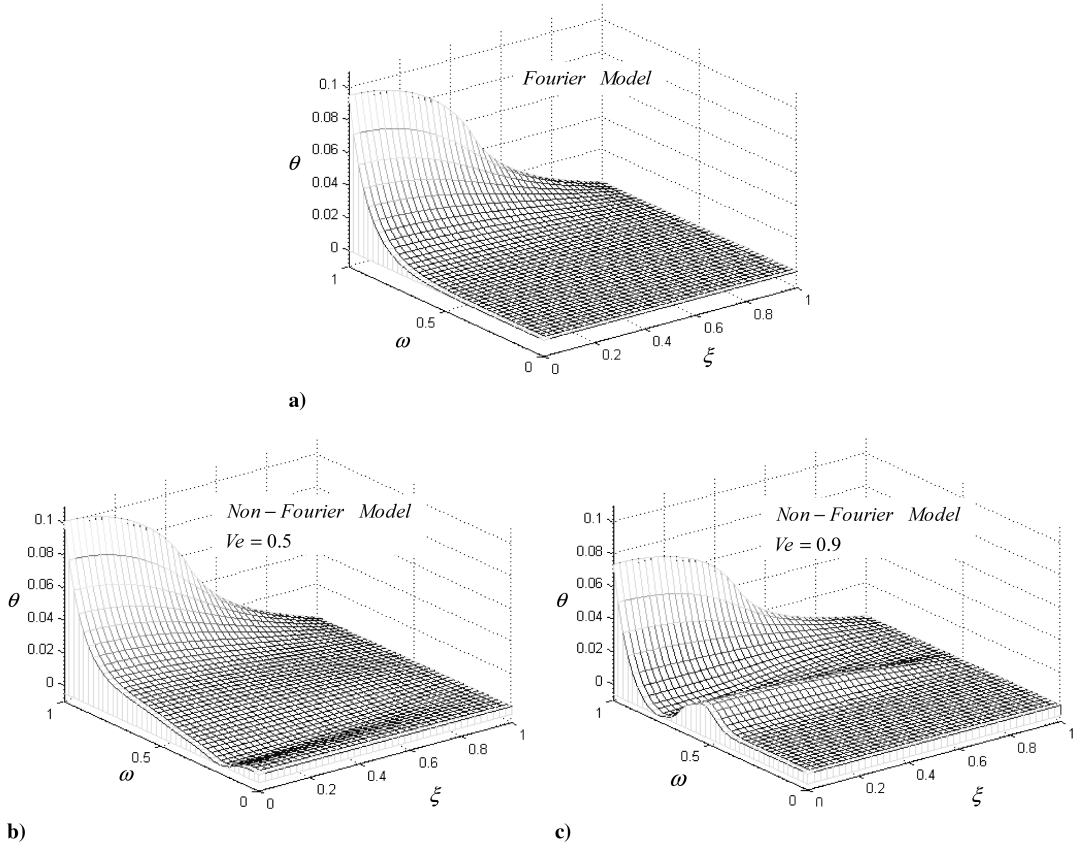

Fig. 7 Surface temperature evolution for both Fourier and non-Fourier models with $Fo = 0.5$, $\xi_1 = 0.5$, and $M = 16$.

Using Eq. (15f) and the orthogonality condition, we find the following:

$$C_{fg} = \frac{-a_f \int_0^1 \sinh(\gamma_f \omega) \sin(\eta_g \omega)\, d\omega}{\int_0^1 \sin^2(\eta_g \omega)\, d\omega} \tag{44}$$

Finally,

$$C_{fg} = -4 \frac{\xi_1 J_1[(\gamma_f/\sqrt{M})\xi_1]\sqrt{M}}{\gamma_f [J_1(\gamma_f/\sqrt{M})]^2} \frac{(-1)^g}{(\eta_g^2 + \gamma_f^2)} \tag{45}$$

As a good comparison, we should solve the same problem with the parabolic heat conduction equation. If Fourier's law holds (i.e., in the limit when $Ve \to 0$), the values of $(\kappa_{g,f})_i$ are always real; therefore, $\psi(\xi, \omega, Fo)$ becomes

$$\psi(\xi, \omega, Fo) = \sum_{f=1}^{\infty} \sum_{g=0}^{\infty} C_{fg} \exp(-\vartheta_{g,f}^2 Fo) \sin(\eta_g \omega) J_0\left(\frac{\gamma_f}{\sqrt{M}} \xi\right) \tag{46}$$

IV. Numerical Solution

To solve this problem numerically, Eq. (8) should be discretized. The discretization can be done in many ways, such as using the finite element method or the control volume method. In this work, we adopted an implicit FDM. In implicit methods, the finite difference approximations of the individual exact partial derivatives in the partial differential equation are evaluated at the solution time level $n + 1$. Implicit schemes are unconditionally stable for any time step, but the accuracy of the solution is only first order in time. The forward difference representation is used for the time derivative, and the central difference representation is used for spatial derivatives. As a result, Eq. (8) can be discretized as follows:

$$\begin{aligned} Ve^2 \frac{\theta_{i,j}^{n+1} - 2\theta_{i,j}^{n} + \theta_{i,j}^{n-1}}{\Delta Fo^2} + \frac{\theta_{i,j}^{n+1} - \theta_{i,j}^{n}}{\Delta Fo} \\ = M\left(\frac{\theta_{i+1,j}^{n+1} - 2\theta_{i,j}^{n+1} + \theta_{i-1,j}^{n+1}}{\Delta \xi^2} + \frac{\theta_{i+1,j}^{n+1} - \theta_{i-1,j}^{n+1}}{2\xi_{i,j}\Delta \xi}\right) \\ + \frac{\theta_{i,j+1}^{n+1} - 2\theta_{i,j}^{n+1} + \theta_{i,j-1}^{n+1}}{\Delta \omega^2} + E_{i,j}^{n} \end{aligned} \tag{47}$$

where [35]

$$\begin{aligned} E_{i,j}^{n} = Ve^2 \frac{\Delta Fo^2}{12} \frac{\partial^4 \theta}{\partial Fo^4} + \frac{\Delta Fo}{2} \frac{\partial^2 \theta}{\partial Fo^2} - M \frac{\Delta \xi^2}{12} \frac{\partial^4 \theta}{\partial \xi^4} \\ - \frac{M \Delta \xi^2}{6\xi} \frac{\partial^3 \theta}{\partial \xi^3} - \frac{\Delta \omega^2}{12} \frac{\partial^4 \theta}{\partial \omega^4} \end{aligned} \tag{48}$$

It is clear that as ΔFo, $\Delta \xi$, and $\Delta \omega$ tend to zero, $E_{i,j}^{n}$ tends to zero and the finite difference approximation [Eq. (47)] satisfies the consistency condition [35].

After neglecting the error term $E_{i,j}^{n}$ and rearranging Eq. (47), the difference equation becomes

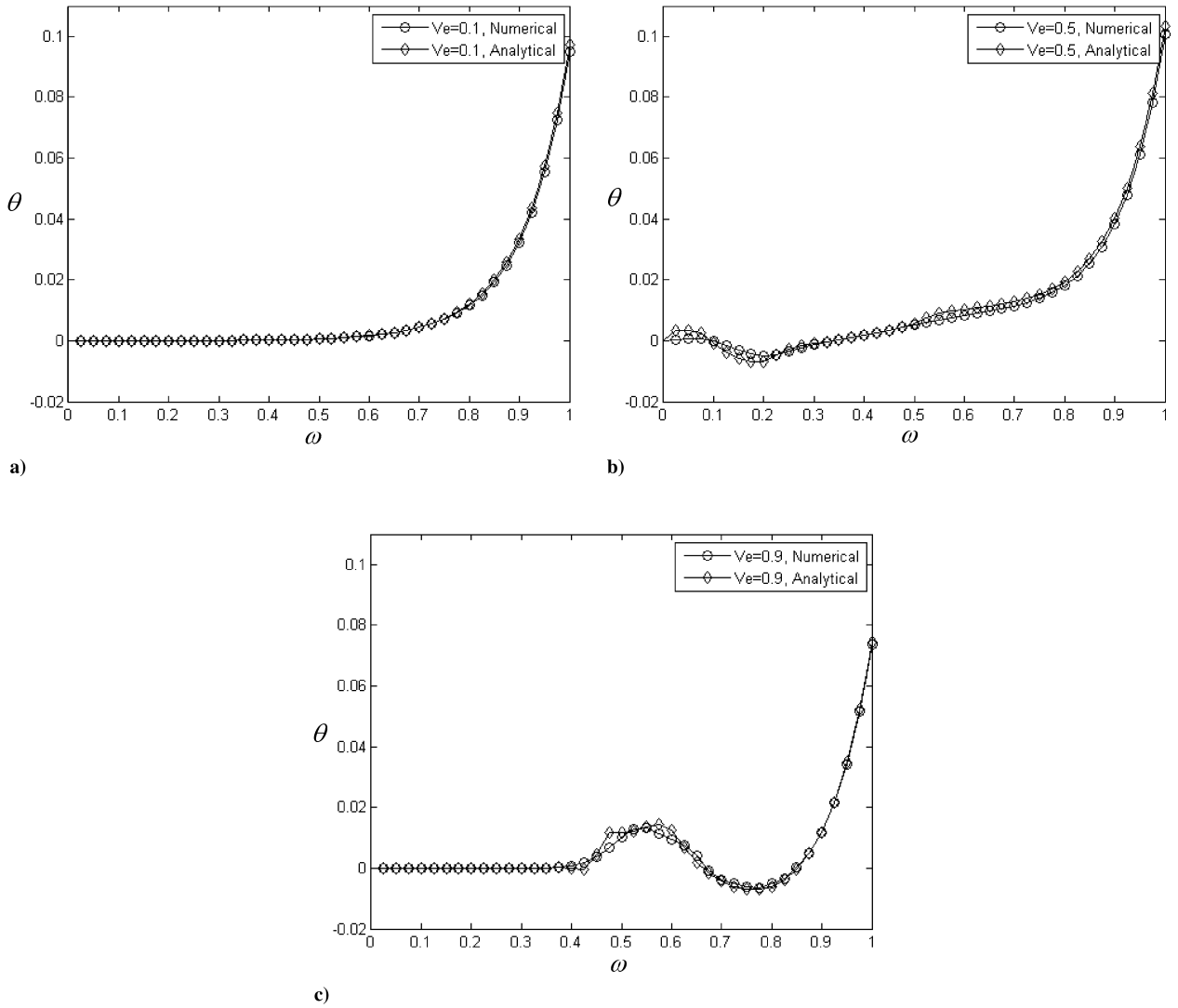

Fig. 8 Distribution for the non-Fourier model along the ω direction with $\xi = 0$, $Fo = 0.5$, $\xi_1 = 0.5$, and $M = 16$.

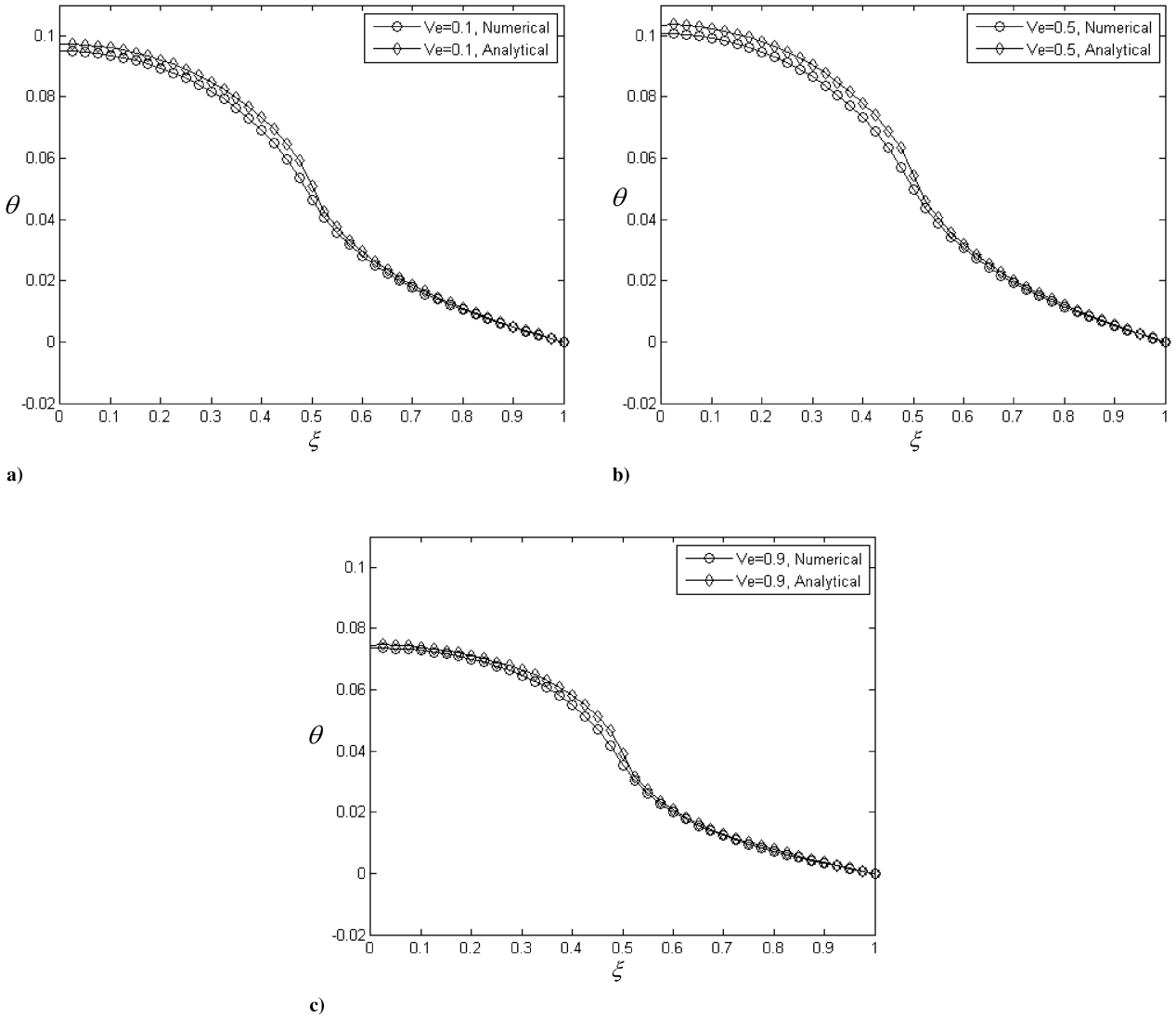

Fig. 9 Distribution for the non-Fourier model along the ξ direction with $\omega = 1$, $Fo = 0.5$, $\xi_1 = 0.5$, and $M = 16$.

Table 2 Errors of the numerical solution compared with the analytical solution

Figure number	Maximum error	Percentage of maximum error	Node coordinates	
			ξ	ω
4b	0.0052	13.0704	0.475	1
4d	0.0067	36.8991	0.05	0.675
4f	0.0052	9.6033	0.475	1
5b	0.0032	30.4016	0.125	1
5d	0.0037	34.5385	0.125	1
5f	0.0034	35.0058	0.125	1
6b	0.0095	28.3220	0.5	1
6d	0.0140	10.4970	0.5	1
6f	0.0170	9.0114	0.5	1
8a	0.0022	3.0197	0	0.975
8b	0.0028	3.5450	0	0.975
8c	0.0047	41.3437	0	0.475
9a	0.0057	9.6525	0.475	1
9b	0.0062	9.8120	0.475	1
9c	0.0049	10.5379	0.475	1

$$\left[\frac{Ve^2}{\Delta Fo^2}+\frac{1}{\Delta Fo}+\frac{2M}{\Delta\xi^2}+\frac{2}{\Delta\omega^2}\right]\theta_{i,j}^{n+1}+\left[-\frac{M}{\Delta\xi^2}+\frac{M}{2\xi_{i,j}\Delta\xi}\right]\theta_{i-1,j}^{n+1}$$
$$+\left[-\frac{M}{\Delta\xi^2}-\frac{M}{2\xi_{i,j}\Delta\xi}\right]\theta_{i+1,j}^{n+1}+\frac{-1}{\Delta\omega^2}(\theta_{i,j+1}^{n+1}+\theta_{i,j-1}^{n+1})$$
$$=\left[\frac{2Ve^2}{\Delta Fo^2}+\frac{1}{\Delta Fo}\right]\theta_{i,j}^{n}+\left[\frac{Ve^2}{\Delta Fo^2}\right]\theta_{i,j}^{n-1} \tag{49}$$

In our treatment, we assume $\Delta\xi=\Delta\omega$. Hence, Eq. (49) leads to the following difference equation:

$$\left[\frac{Ve^2}{\Delta Fo^2}+\frac{1}{\Delta Fo}+\frac{2M}{\Delta\xi^2}+\frac{2}{\Delta\xi^2}\right]\theta_{i,j}^{n+1}+\left[-\frac{M}{\Delta\xi^2}+\frac{M}{2\xi_{i,j}\Delta\xi}\right]\theta_{i-1,j}^{n+1}$$
$$+\left[-\frac{M}{\Delta\xi^2}-\frac{M}{2\xi_{i,j}\Delta\xi}\right]\theta_{i+1,j}^{n+1}+\frac{-1}{\Delta\xi^2}(\theta_{i,j+1}^{n+1}+\theta_{i,j-1}^{n+1})$$
$$=\left[\frac{2Ve^2}{\Delta Fo^2}+\frac{1}{\Delta Fo}\right]\theta_{i,j}^{n}+\left[\frac{Ve^2}{\Delta Fo^2}\right]\theta_{i,j}^{n-1} \tag{50}$$

The preceding system of linear algebraic equations can be written in matrix form as

$$[A_1]\{\theta\}^{n+1}=[B_1]\{\theta\}^{n}+[C_1]\{\theta\}^{n-1} \tag{51}$$

where $[A_1]$ is a five-diagonal matrix, and $[B_1]$ and $[C_1]$ are just diagonal matrices.

At the center, $\xi=0$, we have

$$\lim_{\xi\to 0}\left(\frac{\partial\theta}{\xi\partial\xi}\right)=\frac{\partial^2\theta}{\partial\xi^2}$$

by L'Hôpital's rule. Then, Eq. (8) takes the form

$$Ve^2\frac{\partial^2\theta}{\partial Fo^2}+\frac{\partial\theta}{\partial Fo}=2M\frac{\partial^2\theta}{\partial\xi^2}+\frac{\partial^2\theta}{\partial\omega^2} \tag{52}$$

Hence, Eq. (52) should be discretized for $\xi=0$.

By using matrix inversion, the dimensionless temperature distribution at each time step can be determined. The following numerical solutions correspond to a mesh size of $\Delta\xi=0.025$ and $\Delta Fo=0.001$.

A detailed flowchart of the numerical solution for the cylinder's temperature profile is shown in Fig. 2.

V. Results and Discussion

Using our solution, we performed sample numerical computations of temperature contours and profiles in the cylinder for the heat source form shown in Fig. 1, based on Eqs. (11), (25), and (43) and the numerical solution. These calculations were obtained for $\xi_1=0.1$ or $\xi_1=0.5$, and $M=2$ or $M=16$. The results of the calculations are presented in Figs. 3–12.

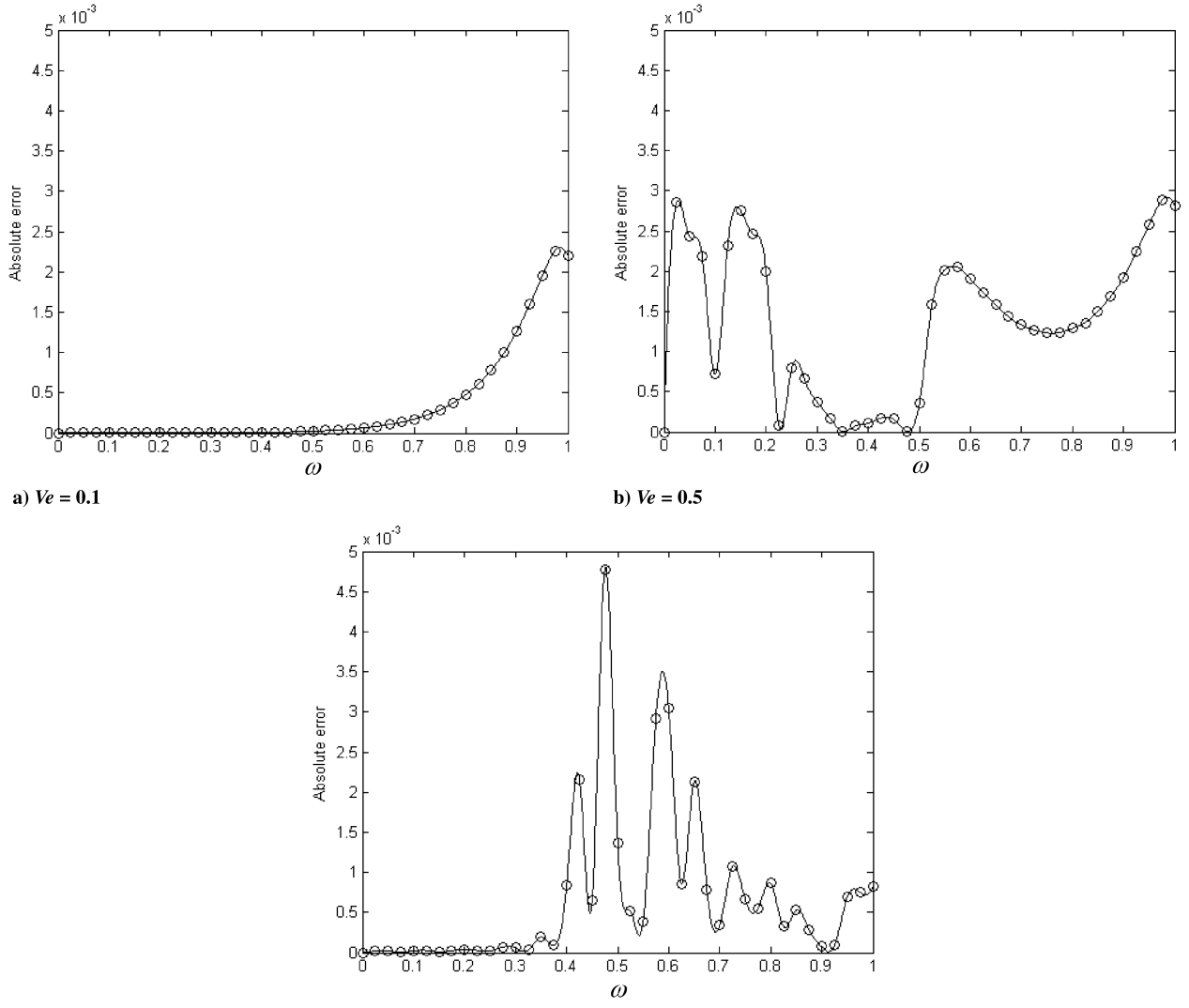

a) *Ve* = 0.1

b) *Ve* = 0.5

c) *Ve* = 0.9

Fig. 10 Absolute error of θ results between the numerical and analytical methods for the non-Fourier model along the ω direction with $\xi=0$, $Fo=0.5$, $\xi_1=0.5$, and $M=16$.

Figure 3 shows convergence of the temperature for a specific point. In this figure, the temperature for the center point of the cylinder was calculated using different numbers of series terms in the calculations. It can be observed from Fig. 3 that, after using 350 values of η_g and 35 values of β_n and γ_f in the calculations, the temperature for this point stabilized, and there is no oscillation in both figures. Therefore, in all calculations, the first 35 values of β_n and γ_f and the first 350 values of η_g were used.

Figure 4 shows temperature field distribution for three nondimensional times. The Vernotte number that we used in the simulation was 0.7. In this simulation, ξ_1 and M were 0.5 and 16, respectively. It can be observed from Fig. 4 that, because of the non-Fourier effect, the thermal wave has not touched the other side of the cylinder at $Fo = 0.5$. Furthermore, thermal waves can be seen clearly in Fig. 4. In addition, negative temperatures can be observed in this figure. Per the previously cited literature [16,17], if hyperbolic heat conduction were a theory based on the local equilibrium hypotheses, as the parabolic heat conduction is, this behavior would represent a violation of the second law of thermodynamics. Indeed, Jou et al. [17] pointed out that hyperbolic heat conduction is in contradiction with the local equilibrium hypothesis, so that no violation of principles of thermodynamics occurs.

Figure 5 shows temperature field distribution for three nondimensional times. The Vernotte number and M that we used in the simulation were the same as those of the previous figure, but ξ_1 was 0.1. A thermal wave can be observed clearly in this figure, although the thermal wave effect is less intense. It is obvious that, because ξ_1 in Fig. 5 is less than that of the previous figure, the dimensionless temperature for the same Fourier number in this figure is less than the dimensionless temperature in the previous figure. However, it is interesting to note that, due to the thermal waves in Figs. 4 and 5 moving at the same speed, the distances spanned by the thermal waves for each nondimensional time in these figures along the ω direction are equal.

In Fig. 6, the distributions for the temperature fields for three nondimensional times are presented. The Vernotte number that we used in the simulation was again 0.7, but ξ_1 and M were 0.5 and 2, respectively. The movement of the thermal wave can clearly be observed in Fig. 6. It is obvious that, because M in Fig. 6 is much less than this parameter in Fig. 4, higher temperatures result in Fig. 6 as compared with those of Fig. 4. In other words, in this figure, the height of the cylinder is almost one-third of the height of the height of the cylinder in Fig. 4; therefore, applying the same heat flux to these two different cylinders causes higher temperatures for the cylinder with lower

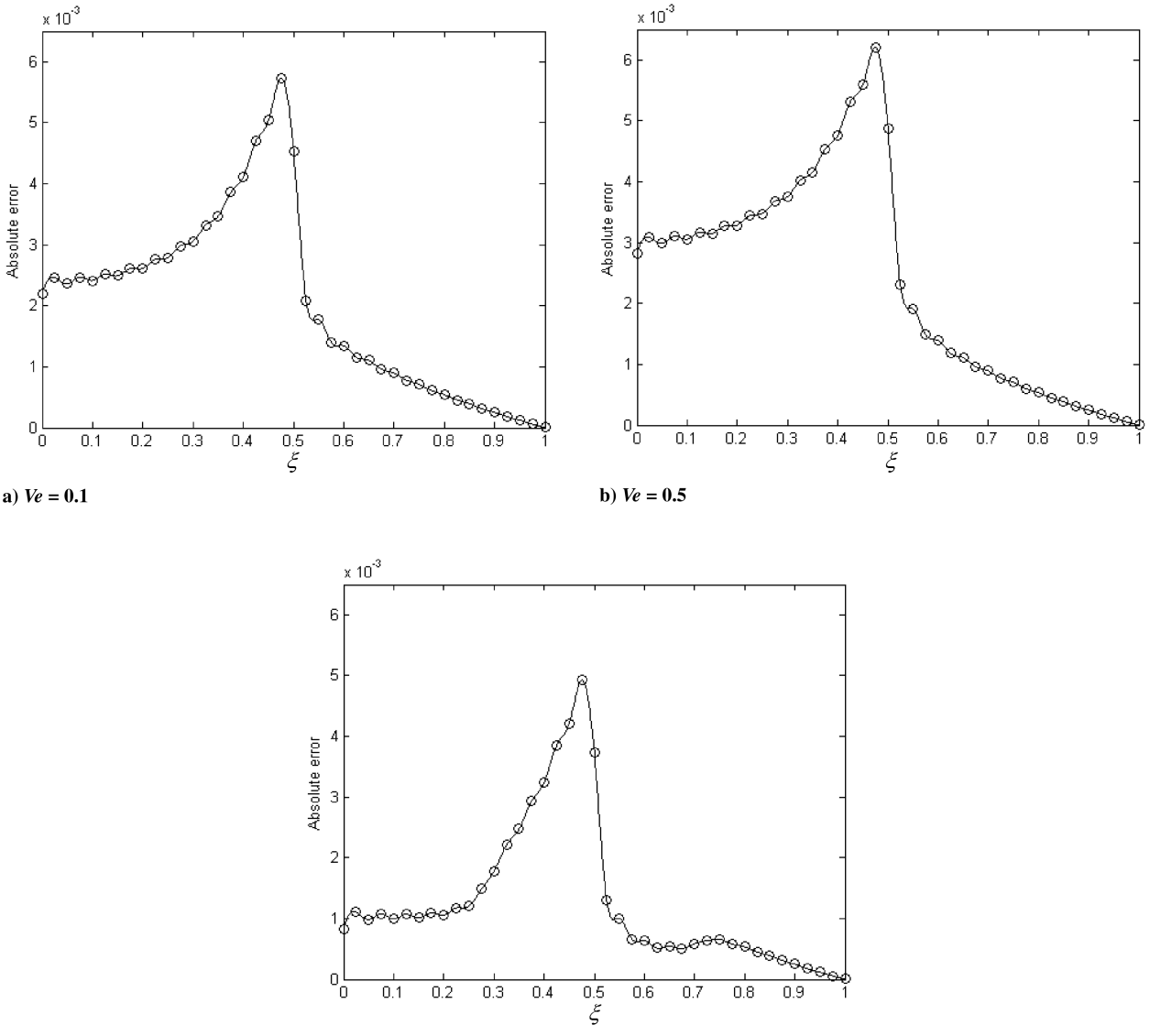

Fig. 11 Absolute error of θ results between the numerical and analytical methods for the non-Fourier model along the ξ direction with $\omega = 1$, $Fo = 0.5$, $\xi_1 = 0.5$, and $M = 16$.

height. Also, it is interesting that, due to use of the same Vernotte numbers in Figs. 4–6, the distances spanned by the thermal waves are equal for each nondimensional time in both numerical and analytical figures along the ω direction. Moreover, it is worth noting that, by neglecting the error term $E_{i,j}^{n}$ in the numerical solution, an artificial viscosity was added to the problem, which makes all of the numerical solutions smoother than the analytical solutions.

In Fig. 7, the distributions for the temperature fields for both the Fourier and non-Fourier models are presented. This figure manifestly shows the difference between the Fourier and non-Fourier models. It can be seen from Fig. 7 that the distributions for the temperature fields in the Fourier model are smooth and without fluctuation. But thermal waves can be observed in the temperature fields for the non-Fourier model.

Figure 8 shows the temperature profiles along the ω direction. This figure shows that, due to the non-Fourier effect, the temperatures at many points in the object remain constant before the wave reaches these locations. This interesting behavior can be observed in all previous figures. It can be deduced from this figure that a cylinder with a lower Vernotte number reaches its equilibrium temperature distribution sooner than a cylinder with a larger Vernotte number. From a physical point of view, this means that, as the speed of the thermal wave increases, the object can reach its equilibrium temperature distribution sooner. Also, because of the fact that a larger thermal relaxation time causes thermal waves with more energy and longer lifetimes, a cylinder with a larger Vernotte number needs more time for disappearance of its thermal wave and to reach its equilibrium temperature distribution.

Figure 9 shows temperature profiles along the ξ axis. The maximum calculated errors are provided in Table 2 for Figs. 4–9. Moreover, the absolute error of dimensionless temperature for the numerical method along the ω and ξ directions are shown in Figs. 10 and 11, respectively. It can be seen from these two figures that, along the ω direction, maximum absolute error occurs when $Ve = 0.9$ is used, However, along the ξ direction, maximum absolute error occurs when $Ve = 0.5$ is used. Hence, it can be deduced that, although our numerical method is accurate in most cases, it has up to a 40% error in some cases (Table 2). To improve the numerical

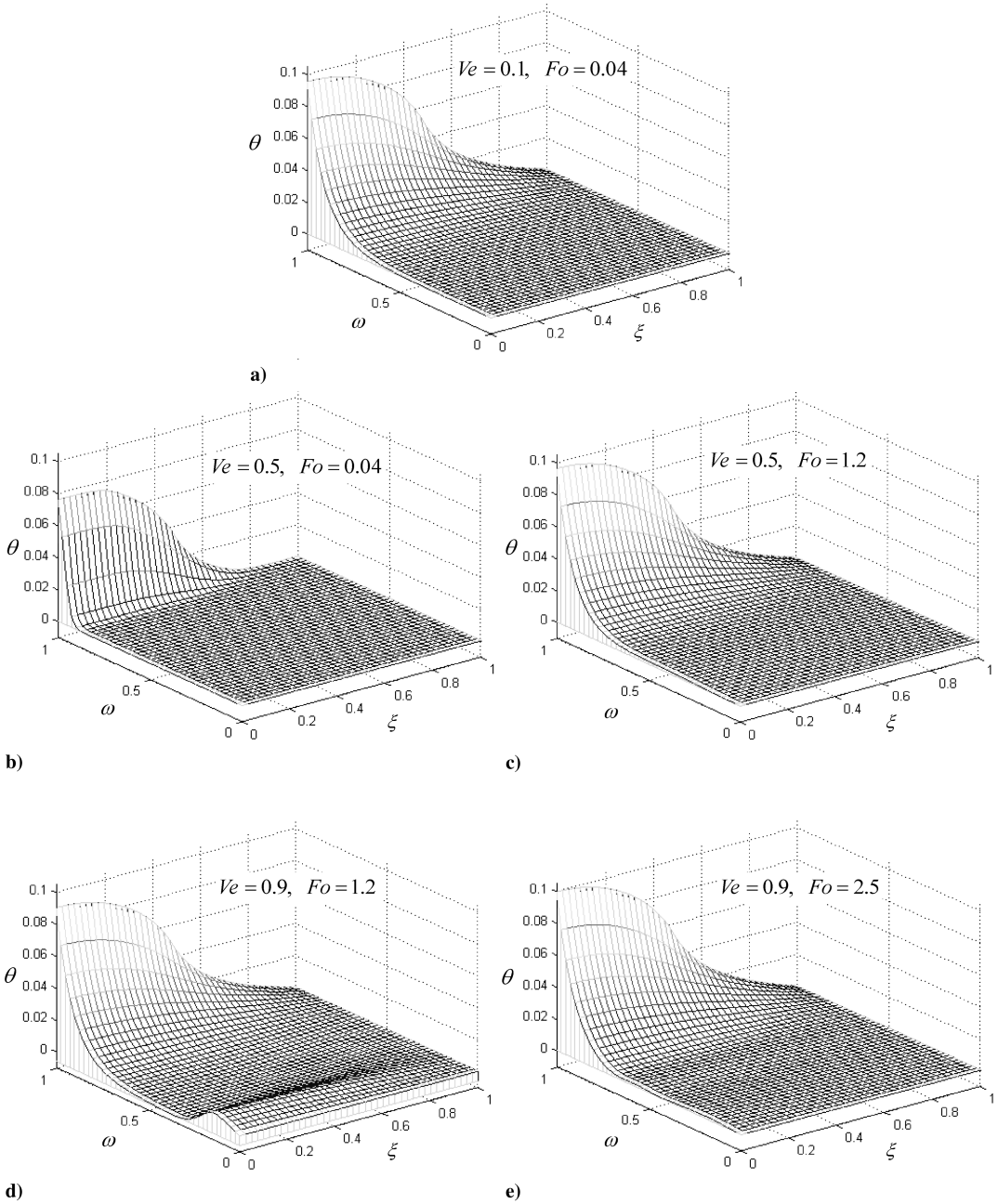

Fig. 12 Surface temperature evolution with different Fourier and Vernotte numbers for the non-Fourier model numerical result with $\xi_1 = 0.5$ and $M = 16$.

method, higher-order approximations should be used to reduce the error term of the Taylor approximation. The present analytical solution provides a useful tool to calculate the error of numerical solutions for the HHCE.

Figure 12 shows surface temperature profiles for five cases using the numerical method. It is observed that, as the Vernotte number increases, the time that the whole cylinder needs in order to reach the equilibrium temperature distribution increases. Comparing Fig. 12a with Fig. 12b, it can be found that, when $Ve = 0.5$ is used instead of $Ve = 0.1$, the whole cylinder does not reach its equilibrium temperature distribution and needs more time to reach its equilibrium temperature distribution. Accordingly, by comparing Fig. 12c with Fig. 12d, similar results can be found.

VI. Conclusions

In this paper, the two-dimensional HHCE was solved analytically and numerically for the case of a cylinder. The separation of variables method was employed for the analytical solution, and the implicit FDM was employed for the numerical solution. Eight different examples have been presented. We observe that, although our numerical method is accurate at most points, it has up to a 40% error at some points. Also, we deduce that the larger the Vernotte number, the longer it takes for a point to sense the thermal wave. We also see that, the larger the Vernotte number, the longer it takes for the cylinder to reach its equilibrium temperature distribution. In other words, larger thermal relaxation time causes the thermal wave to move with a lower speed and more energy; therefore, it needs more time to reach a specific point in the object. Also, because of the fact that larger thermal relaxation time results in a thermal wave with more energy and longer lifetime, the object needs more time for the disappearance of thermal waves and to reach equilibrium temperature distribution.

Acknowledgments

This work is supported by the Department of Mechanical Engineering and the talented office of Semnan University. The authors also thank the referees for their constructive comments on the manuscript.

References

[1] Özisik, M. N., *Finite Difference Methods in Heat Transfer*, CRC Press, Boca Raton, FL, 1994.

[2] Liu, H., Bussmann, M., and Mostaghimi, J., "A Comparison of Hyperbolic and Parabolic Models of Phase Change of a Pure Metal," *International Journal of Heat and Mass Transfer*, Vol. 52, Nos. 5–6, 2009, pp. 1177–1184. doi:10.1016/j.ijheatmasstransfer.2008.08.030

[3] Niu, T., and Dai, W., "A Hyperbolic Two-Step Model Based Finite Difference Scheme for Studying Thermal Deformation in a Double-Layered Thin Film Exposed to Ultrashort-Pulsed Lasers," *International Journal of Thermal Sciences*, Vol. 48, No. 1, 2009, pp. 34–49. doi:10.1016/j.ijthermalsci.2008.02.001

[4] Lewandowska, M., and Malinowski, L., "Analytical Method for Determining Critical Energies of Uncooled Superconductors Based on the Hyperbolic Model of Heat Conduction," *Cryogenics*, Vol. 41, No. 4, 2001, pp. 267–273. doi:10.1016/S0011-2275(01)00094-7

[5] Tung, M. M., Trujillo, M., Molina, J. A. L., Rivera, M. J., and Berjano, E. J., "Modeling the Heating of Biological Tissue Based on the Hyperbolic Heat Transfer Equation," *Mathematical and Computer Modelling*, Vol. 50, Nos. 5–6, 2009, pp. 665–672. doi:10.1016/j.mcm.2008.12.023

[6] Cattaneo, C., "Sur une Forme de l'Equation de la Chaleur Eliminant le Paradoxe d'Une Propagation Instantanée," *Comptes Rendus de l'Académie des Sciences*, Vol. 247, 1958, pp. 431–433.

[7] Vernotte, P., "Les Paradoxes de la Théorie Continue de l'Equation de la Chaleur," *Comptes Rendus de l'Académie des Sciences*, Vol. 246, 1958, pp. 3154–3155.

[8] Shen, W., and Han, S., "A Numerical Solution of Two-Dimensional Hyperbolic Heat Conduction with Non-Linear Boundary Conditions," *Heat and Mass Transfer*, Vol. 39, Nos. 5–6, 2003, pp. 499–507. doi:10.1007/s00231-003-0414-3

[9] Jackson, H. E., and Walker, C. T., "Thermal Conductivity, Second Sound, and Phonon–Phonon Interactions in NaF," *Physical Review B*, Vol. 3, No. 4, 1971, pp. 1428–1439. doi:10.1103/PhysRevB.3.1428

[10] Narayanamurti, V., and Dynes, R. C., "Observation of Second Sound in Bismuth," *Physical Review Letters*, Vol. 28, No. 22, 1972, pp. 1461–1465. doi:10.1103/PhysRevLett.28.1461

[11] Zhou, J., Zhang, Y., and Chen, J. K., "An Axisymmetric Dual-Phase-Lag Bioheat Model for Laser Heating of Living Tissues," *International Journal of Thermal Sciences*, Vol. 48, No. 8, 2009, pp. 1477–1485. doi:10.1016/j.ijthermalsci.2008.12.012

[12] Zhou, J., Chen, J. K., and Zhang, Y., "Dual-Phase-Lag Effects on Thermal Damage to Biological Tissues Caused by Laser Irradiations," *Computers in Biology and Medicine*, Vol. 39, No. 3, 2009, pp. 286–293. doi:10.1016/j.compbiomed.2009.01.002

[13] Xu, F., Seffen, K. A., and Liu, T. J., "Non-Fourier Analysis of Skin Biothermomechanics," *International Journal of Heat and Mass Transfer*, Vol. 51, Nos. 9-10, 2008, pp. 2237–2259. doi:10.1016/j.ijheatmasstransfer.2007.10.024

[14] Korner, C., and Bergmann, H. W., "The Physical Defects of the Hyperbolic Heat Conduction Equation," *Applied Physics, A: Materials Science and Processing*, Vol. 67, No. 4, 1998, pp. 397–401. doi:10.1007/s003390050792

[15] Al-Nimr, M., and Naji, M., "On the Phase-Lag Effect on the Nonequilibrium Entropy Production," *Microscale Thermophysical Engineering*, Vol. 4, No. 4, 2000, pp. 231–243. doi:10.1080/108939500300005403

[16] Galovic, S., Kostoski, D., Stamboliev, G., and Suljovrujic, E., "Thermal Wave Propagation in Media with Thermal Memory Induced by Pulsed Laser Irradiation," *Radiation Physics and Chemistry*, Vol. 67, Nos. 3–4, 2003, pp. 459–461. doi:10.1016/S0969-806X(03)00085-9

[17] Jou, D., Casas-Vazquez, J., and Lebon, G., "Extended Irreversible Thermodynamics," *Reports on Progress in Physics*, Vol. 51, No. 8, 1988, pp. 1105–1179. doi:10.1088/0034-4885/51/8/002

[18] López Molina, J. A., Rivera, M. J., Trujillo, M., and Berjano, E. J., "Thermal Modeling for Pulsed Radio Frequency Ablation: Analytical Study Based on Hyperbolic Heat Conduction," *Medical Physics*, Vol. 36, No. 4, 2009, pp. 1112–1119. doi:10.1118/1.3085824

[19] Lewandowska, M., and Malinowski, L., "An Analytical Solution of the Hyperbolic Heat Conduction Equation for the Case of a Finite Medium Symmetrically Heated on Both Sides," *International Communications in Heat and Mass Transfer*, Vol. 33, No. 1, 2006, pp. 61–69. doi:10.1016/j.icheatmasstransfer.2005.08.004

[20] Moosaie, A., "Non-Fourier Heat Conduction in a Finite Medium with Arbitrary Source Term and Initial Conditions," *Forschung im Ingenieurwesen / Verein Deutscher Ingenieure*, Vol. 71, Nos. 3-4, 2007, pp. 163–169. doi:10.1007/s10010-007-0054-8

[21] Moosaie, A., "Non-Fourier Heat Conduction in a Finite Medium with Insulated Boundaries and Arbitrary Initial Conditions," *International Communications in Heat and Mass Transfer*, Vol. 35, No. 1, 2008, pp. 103–111. doi:10.1016/j.icheatmasstransfer.2007.08.001

[22] Tang, D. W., and Araki, N., "Non-Fourier Heat Conduction in a Finite Medium under Periodic Surface Thermal Disturbance," *International Journal of Heat and Mass Transfer*, Vol. 39, No. 8, 1996, pp. 1585–1590. doi:10.1016/0017-9310(95)00261-8

[23] Zhang, D., Li, L., Li, Z., Guan, L., and Tan, X., "Non-Fourier Conduction Model with Thermal Source Term of Ultra Short High Power Pulsed Laser Ablation and Temperature Evolvement Before Melting," *Physica B, Condensed Matter*, Vol. 364, Nos. 1–4, 2005, pp. 285–293. doi:10.1016/j.physb.2005.04.025

[24] Saleh, A., and Al-Nimr, M., "Variational Formulation of Hyperbolic Heat Conduction Problems Applying Laplace Transform Technique," *International Communications in Heat and Mass Transfer*, Vol. 35, No. 2, 2008, pp. 204–214. doi:10.1016/j.icheatmasstransfer.2007.06.010

[25] Jiang, F. M., and Sousa, A. C. M., "Analytical Solution for Hyperbolic Heat Conduction in a Hollow Sphere," *Journal of Thermophysics and Heat Transfer*, Vol. 19, No. 4, 2005, pp. 595–598. doi:10.2514/1.13472

[26] Barletta, A., and Zanchini, E., "Three-Dimensional Propagation of Hyperbolic Thermal Waves in a Solid Bar with Rectangular Cross-Section," *International Journal of Heat and Mass Transfer*, Vol. 42, No. 2, 1999, pp. 219–229. doi:10.1016/S0017-9310(98)00190-2

[27] Chen, H. T., and Lin, J. Y., "Numerical Analysis for Hyperbolic Heat Conduction," *International Journal of Heat and Mass Transfer*, Vol. 36, No. 11, 1992, pp. 2891–2898. doi:10.1016/0017-9310(93)90108-I

[28] Yang, C. Y., "Direct and Inverse Solutions of Hyperbolic Heat Conduction Problems," *Journal of Thermophysics and Heat Transfer*, Vol. 19, No. 2, 2005, pp. 217–225. doi:10.2514/1.7410

[29] Zhou, J., Zhang, Y., and Chen, J. K., "Non-Fourier Heat Conduction Effect on Laser-Induced Thermal Damage in Biological Tissues," *Numerical Heat Transfer, Part A: Applications*, Vol. 54, No. 1, 2008, pp. 1–19. doi:10.1080/10407780802025911

[30] Huang, C. H., and Lin, C. Y., "Inverse Hyperbolic Conduction Problem in Estimating Two Unknown Surface Heat Fluxes Simultaneously," *Journal of Thermophysics and Heat Transfer*, Vol. 22, No. 4, 2008, pp. 766–774. doi:10.2514/1.36331

[31] Yang, C. Y., "Direct and Inverse Solutions of the Two-Dimensional Hyperbolic Heat Conduction Problems," *Applied Mathematical Modelling*, Vol. 33, No. 6, 2009, pp. 2907–2918. doi:10.1016/j.apm.2008.10.001

[32] Babaei, M. H., and Chen, Z., "Transient Hyperbolic Heat Conduction in a Functionally Graded Hollow Cylinder," *Journal of Thermophysics and Heat Transfer*, Vol. 24, No. 2, 2010, pp. 325–330. doi:10.2514/1.41368

[33] Carslaw, H. S., and Jaeger, J. C., *Conduction of Heat in Solids*, 2nd ed., Oxford Univ. Press, New York, 2000.

[34] Özisik, M. N., *Heat Conduction*, 2nd ed., Wiley, New York, 1993.

[35] Hoffman, J. D., *Numerical Methods for Engineers and Scientists*, 2nd ed., CRC Press, New York, 2001.